Shear Modulus and Shear-Stress Fluctuations in Polymer Glasses

I. Kriuchevskyi, J. P. Wittmer,* H. Meyer, and J. Baschnagel
Institut Charles Sadron, Université de Strasbourg and CNRS, 23 rue du Loess, 67034 Strasbourg Cedex, France
(Received 26 May 2017; revised manuscript received 14 August 2017; published 4 October 2017)

Using molecular dynamics simulation of a standard coarse-grained polymer glass model, we investigate by means of the stress-fluctuation formalism the shear modulus μ as a function of temperature T and sampling time Δt. While the ensemble-averaged modulus $\mu(T)$ is found to decrease continuously for all Δt sampled, its standard deviation $\delta\mu(T)$ is nonmonotonic, with a striking peak at the glass transition. Confirming the effective time-translational invariance of our systems, $\mu(\Delta t)$ can be understood using a weighted integral over the shear-stress relaxation modulus $G(t)$. While the crossover of $\mu(T)$ gets sharper with an increasing Δt, the peak of $\delta\mu(T)$ becomes more singular. It is thus elusive to predict the modulus of a single configuration at the glass transition.

DOI: 10.1103/PhysRevLett.119.147802

Introduction.—The shear modulus μ is the central, mechanically directly accessible order parameter characterizing the transition from the liquid-sol ($\mu = 0$) to the solid-gel state ($\mu > 0$) [1–5]. Since the shear modulus $\mu(T)$ of crystalline solids vanishes discontinuously at the melting point with an increasing temperature T [6], this begs the question of the behavior of $\mu(T)$ for amorphous solids near the glass transition temperature T_g [6–16]. Two qualitatively different scenarios have been put forward, being in favor either of a *continuous* (cusplike) transition [6–10] or of a *discontinuous* jump at T_g [11–16]. The jump singularity is a result of mean-field theories [11,16,17], which find the energy barriers for complete structural relaxation to diverge at T_g so that liquidlike flow stops. However, in experimental or simulated glass formers, the barriers do not diverge abruptly. Such non-mean-field effects are expected to smear out the sharp transition [16]. Another line of recent research has focused on the elastic properties deep in the glass [18–20]. At $T \ll T_g$ a transition in the solid is found, where multiple particle arrangements occur as different competing glassy states. This so-called Gardner transition is thus accompanied by strong fluctuations of μ from one glass state to the other [19,20]. Interestingly, strong fluctuations of μ were also observed in amorphous self-assembled networks [21] (a model for vitrimers [22]). The results of Refs. [19–21] beg the question of whether the emergence of shear rigidity at the glass transition is also accompanied by strong fluctuations of μ. Here, we address both questions by means of large-scale molecular dynamics (MD) [23] simulations of a standard model for glassy polymers [24–28]. Details about the model, the quench protocol, and the measured observables may be found in the Supplemental Material (SM) [29]. Lennard-Jones units [23] are used below.

Key findings.—Following the pioneering work by Barrat *et al.* [7] and many recent numerical studies [6,10,20,27,28,30–32], we use the stress-fluctuation formalism [33–37] to determine the shear modulus. Our key findings for μ and its standard deviation $\delta\mu$, obtained as a function of T for a broad range of sampling times Δt, are summarized in Fig. 1. Although $\mu(T)$ remains always continuous, it becomes systematically more steplike with an increasing Δt. At variance with the monotonic modulus $\mu(T)$, its standard deviation $\delta\mu(T)$ is nonmonotonic with a remarkable peak near $T_g \approx 0.38$. (As explained in the SM [29], T_g is defined here by means of a Δt-independent dilatometric criterion during the initial continuous temperature quench [6,27].) The peak increases with Δt, becoming about a third of the drop of $\mu(T)$ between $T = 0.34$ and $T = 0.38$ for $\Delta t = 10^5$. The liquid-solid transition is thus

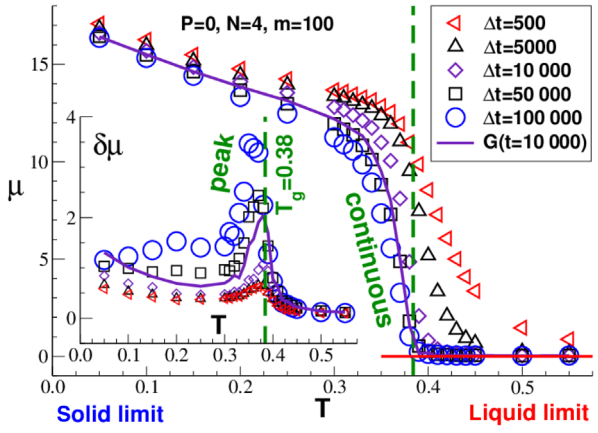

FIG. 1. Key findings as a function of temperature T. The vertical dashed lines indicate the glass transition temperature $T_g \approx 0.38$. (Main panel) Shear modulus $\mu(T)$ for different sampling times Δt showing that the transition becomes more and more steplike with an increasing Δt. (Inset) Corresponding standard deviation $\delta\mu(T)$ showing a peak at $T \approx T_g$ which becomes sharper with an increasing Δt. Also included are the shear-stress relaxation modulus $G(t)$ and its standard deviation $\delta G(t)$ taken at a time $t = 10^4$ (the bold solid lines).

 © 2017 American Physical Society

accompanied by strong fluctuations between different glass configurations. We corroborate these results below. Specifically, we shall trace back the observed Δt dependence of μ to the time dependence of the shear-stress relaxation modulus $G(t)$ [4].

Time series.—Our $m = 100$ independently quenched configurations contain 3072 chains of length $N = 4$. A vanishing normal pressure ($P = 0$) is imposed for all T's. Having reached a specific temperature and after tempering over $\Delta t_{\max} = 10^5$, we perform production runs again over $\Delta t_{\max}$ with entries made each velocity-Verlet sweep. Of importance here are the instantaneous shear stress $\hat{\tau}$ and the instantaneous "affine shear modulus" $\hat{\mu}_A$. As mentioned in Sec. II of the SM [29], $\hat{\tau}$ is the first functional derivative of the Hamiltonian with respect to an imposed infinitesimal canonical and affine shear transformation and $\hat{\mu}_A$ the corresponding second functional derivative [10,21,35–38]. The stored time series are used to compute for a given configuration and shear plane various *time averages* [23] (marked by horizontal bars) over sampling times $\Delta t \leq \Delta t_{\max}$:

$$\bar{\mu}_A \equiv \overline{\hat{\mu}_A}, \tag{1}$$

$$\bar{\mu}_F \equiv \bar{\mu}_0 - \bar{\mu}_1, \quad \text{with} \quad \bar{\mu}_0 \equiv \beta V \overline{\hat{\tau}^2}, \qquad \bar{\mu}_1 \equiv \beta V \bar{\hat{\tau}}^2, \tag{2}$$

$$\bar{\mu} \equiv \bar{\mu}_A - \bar{\mu}_F \equiv (\bar{\mu}_A - \bar{\mu}_0) + \bar{\mu}_1, \tag{3}$$

with $\beta = 1/T$ being the inverse temperature and V the volume of each configuration.

Expectation values.—The corresponding ensemble averages $\mu_A \equiv \langle \bar{\mu}_A \rangle$, $\mu_0 \equiv \langle \bar{\mu}_0 \rangle$, $\mu_1 \equiv \langle \bar{\mu}_1 \rangle$, $\mu_F \equiv \langle \bar{\mu}_F \rangle$, and $\mu \equiv \langle \bar{\mu} \rangle$ are then obtained by averaging over the m configurations and the three shear planes [39]. We have already presented the modulus $\mu(T)$ in the main panel of Fig. 1 using a linear representation. Figure 2 presents $\mu(T)$ and its various contributions for $\Delta t = \Delta t_{\max} = 10^5$ using half-logarithmic coordinates. As emphasized above, although $\mu = \mu_A - \mu_F$ increases rapidly below T_g, the data remain continuous, in line with findings reported for colloidal glass formers [6,7,10] that also use the stress-fluctuation formula. As one expects, $\mu = \mu_1 = 0$ in the liquid limit above T_g, and hence $\mu_F = \mu_0 = \mu_A$ [10,28,35]. At variance to this, $\mu_F < \mu_A$ below T_g; i.e., the shear-stress fluctuations do not have sufficient time to fully explore the phase space. In agreement with Lutsko [34] and more recent studies [6,10,30,31], μ_F does not vanish for $T \to 0$; i.e., μ_A is only an upper bound of $\mu = \mu_A - \mu_F$. We emphasize that while $\mu_F = \mu_0 - \mu_1$ is more or less constant below T_g, its contributions μ_0 and μ_1 increase rapidly with a decreasing T.

Ensemble fluctuations.—To also characterize the fluctuations between different configurations, we take for various properties in addition to the second moment over the ensemble. As already seen in the inset of Fig. 1, we thus compute, e.g., the standard deviation of the shear modulus

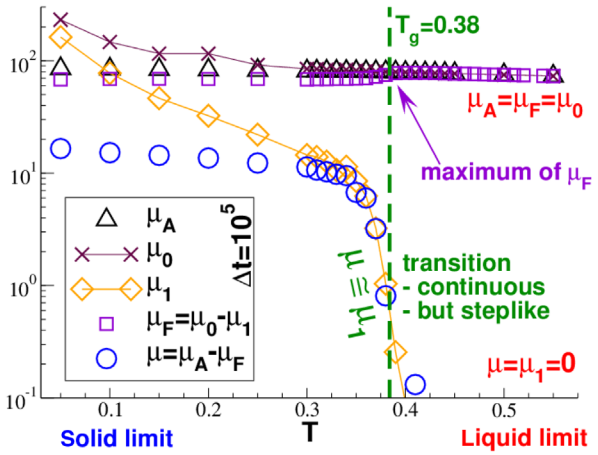

FIG. 2. First moments μ_A, μ_0, μ_1, μ_F, and μ vs temperature T using a half-logarithmic representation. The data are obtained for $\Delta t = \Delta t_{\max} = 10^5$. With decreasing temperature, $\mu \approx \mu_1$ increases rapidly at T_g, but it remains continuous. Interestingly, μ_0 deviates from μ_A and μ_1 from μ below T_g.

$\delta\mu = \sqrt{\langle \bar{\mu}^2 \rangle - \langle \bar{\mu} \rangle^2}$ [39]. $\delta\mu$ is presented together with the corresponding standard deviations $\delta\mu_A$, $\delta\mu_0$, $\delta\mu_1$, and $\delta\mu_F$ in Fig. 3. As can be seen, $\delta\mu_A$ is negligible and $\delta\mu \approx \delta\mu_F$ for all T's. In the high-T regime, we find that $\delta\mu \approx \delta\mu_0$, while $\delta\mu_1 \approx \mu_1$ vanishes much more rapidly. In the opposite glass limit, $\delta\mu \approx \delta\mu_F$ becomes orders of magnitude smaller than $\delta\mu_0 \approx \delta\mu_1$ [28]. The contributions $\bar{\mu}_0$ and $\bar{\mu}_1$ of the difference $\bar{\mu}_F = \bar{\mu}_0 - \bar{\mu}_1$ thus must be strongly correlated, as one verifies using the corresponding correlation coefficient. This is yet another manifestation of the strong frozen shear stresses which are generated in each configuration while quenching the systems through the glass transition.

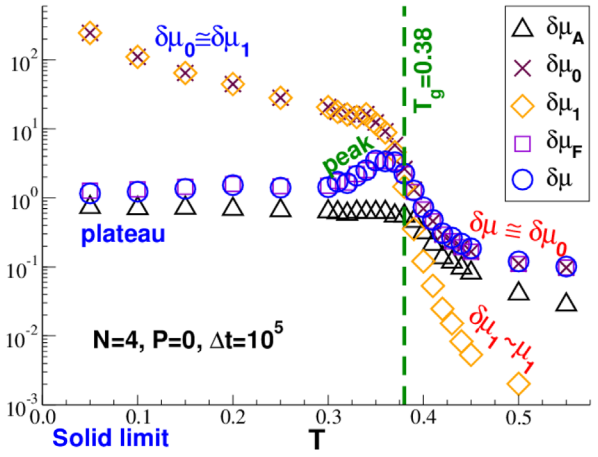

FIG. 3. Standard deviations $\delta\mu_A$, $\delta\mu_0$, $\delta\mu_1$, $\delta\mu_F$, and $\delta\mu$ as a function of T.$\delta\mu_A$ is found to be small, and $\delta\mu \approx \delta\mu_F$ for all T's. Below T_g, the standard deviations $\delta\mu_1$ and $\delta\mu_0$ become rapidly similar and orders of magnitude larger than $\delta\mu_F$. This confirms the presence of strong frozen shear stresses.

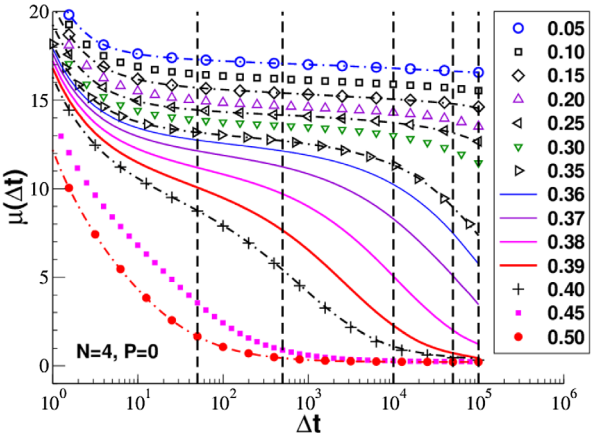

FIG. 4. Shear modulus μ as a function of sampling time Δt for a broad range of T's, as indicated in the figure. $\mu(\Delta t)$ decreases continuously with Δt. Note that a smaller temperature increment $\Delta T = 0.01$ is used around T_g (the solid lines), where $\mu(\Delta t; T)$ changes much more rapidly with T. The dashed-dotted lines are obtained using Eq. (4) by integrating the directly measured shear-stress relaxation modulus $G(t)$. The vertical lines mark the sampling times used in Fig. 1.

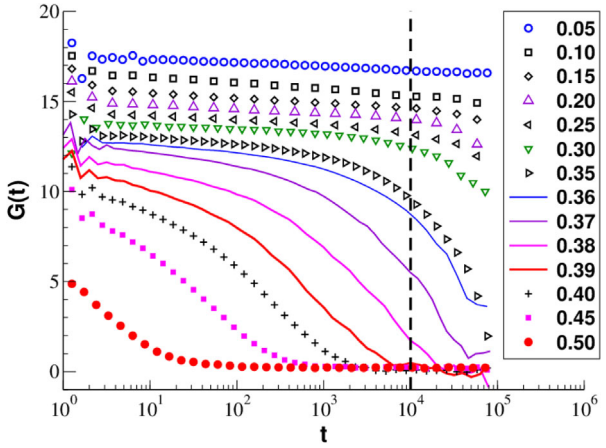

FIG. 5. Stress relaxation modulus $G(t)$ for a broad range of T's. The data are rather similar to the shear modulus $\mu(\Delta t)$ presented in Fig. 4. The dashed vertical line marks the time $t = 10^4$ used for $G(t)$ and $\delta G(t)$ in Fig. 1.

Δt dependence.—We return now to the sampling time dependence shown in Fig. 1. As expected from crystalline and amorphous solids [6,10] and permanent [10,38] and transient [21] elastic networks, the expectation values of the contributions μ_A and μ_0 to μ are strictly Δt independent (not shown). This can be traced back to the fact that their time and ensemble averages commute [38,40]. This is strikingly different for μ_1, μ_F, and μ, for which this commutation relation does not hold. As shown in Fig. 4, we focus here on the Δt dependence of $\mu(\Delta t) = (\mu_A - \mu_0) + \mu_1(\Delta t)$. Covering a broad range of temperatures, we use subsets of length Δt of the total trajectories of length $\Delta t_{\max}$ stored. It is seen that $\mu(\Delta t)$ decreases both monotonically and continuously with Δt. The figure reveals that $\mu(\Delta t; T)$ decreases also monotonically and continuously with T. A glance at Fig. 4 shows that one expects the transition of $\mu(T)$ to get shifted to a lower T and to become more steplike with an increasing Δt, in agreement with Fig. 1. [Note that $\mu(\Delta t)$ increases for $T \to 0$, while its decay slows down.] It is, however, impossible to reconcile the data with a jump singularity at a *finite* Δt and T. Nor is it possible to achieve a reasonable data collapse by shifting the data.

Connection between $\mu(\Delta t)$ and $G(t)$.—The systematic sampling time dependence of $\mu(\Delta t)$ shown in Figs. 1 and 4 can be understood from the generic sampling time dependence of time-averaged fluctuations [41]. Assuming time-translational invariance $\mu(\Delta t)$ may be written as a weighted average [21,28,35–38],

$$\mu(\Delta t) = \frac{2}{\Delta t^2} \int_0^{\Delta t} (\Delta t - t) G(t) dt, \tag{4}$$

over the shear-relaxation modulus $G(t)$ [29]. As shown in Fig. 5, we have computed $G(t)$ directly by means of the fluctuation-dissipation relation appropriate for canonical ensembles with quenched or sluggish shear stresses [28,29,35,38]. Having thus characterized the relaxation modulus $G(t)$, the numerical sum corresponding to Eq. (4) yields the thin dashed-dotted lines indicated in Fig. 4. Being identical with the stress-fluctuation formula $\mu = \mu_A - \mu_F$ for *all* T's, this confirms the assumed time-translational invariance. The Δt dependence of μ, μ_1, and μ_F is thus simply due to the upper boundary Δt used to average $G(t)$. As one expects from Eq. (4) [29], the functional forms of $\mu(\Delta t)$ and $G(t)$ are rather similar, especially at low T. Fixing a time t—say, $t = 10^4$, as indicated by the vertical dashed line in Fig. 5—allows us to characterize the temperature dependence of the relaxation modulus $G(t)$ and its standard deviations $\delta G(t)$ (the bold solid lines in Fig. 1). Consistent with Eq. (4), the behavior found is similar to that of $\mu(T)$ and $\delta\mu(T)$.

Distribution of $\bar{\mu}$.—The striking peak of $\delta\mu$ below T_g seen in Fig. 1 begs for a more detailed characterization of the distribution $p(\bar{\mu}; T, \Delta t)$ of the time-averaged shear modulus $\bar{\mu}$. Focusing on our largest sampling time $\Delta t_{\max}$, the main panel of Fig. 6 presents normalized histograms obtained using $3 \times m = 300$ measurements. We emphasize that the histograms are unimodal for all T's and Δt's [42]. The T dependence of μ and $\delta\mu$ below T_g seen in Fig. 1 is thus not due to, e.g., the superposition of two configuration populations representing solid states with a finite $\bar{\mu}$ and liquid states with $\bar{\mu} \approx 0$. The maximum $\mu_{\max}$ of the (unimodal) distribution systematically shifts to higher values below T_g, in agreement with its first moment μ (Fig. 1), while the distributions become systematically broader and more lopsided; i.e., liquidlike configurations with a small $\bar{\mu}$ remain relevant. The increase of $\delta\mu$ with

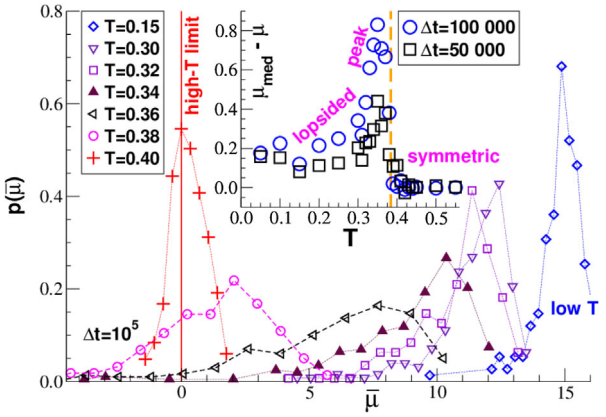

FIG. 6. (Main panel) Distribution $p(\bar{\mu})$ for $\Delta t = 10^5$ for different T's. (Inset) Difference $\mu_{\rm med} - \mu$ of the median $\mu_{\rm med}$ and the ensemble average μ vs T for two sampling times. The difference has a peak slightly below T_g corresponding to very lopsided distributions.

sampling time Δt seen in the inset of Fig. 1 is due to the broadening of $p(\bar{\mu})$ caused by the growing weight of small-$\bar{\mu}$ configurations (not shown). For even smaller temperatures where $T \ll T_g$, the distributions get again more focused around their maxima $\mu_{\rm max}$ (as expected from Fig. 1) and less lopsided. That the large standard deviations and the asymmetry of the distributions are related is demonstrated by comparing the first moment μ of the distribution, its median $\mu_{\rm med}$, and its maximum $\mu_{\rm max}$. One confirms that $0 < \mu_{\rm med} - \mu < \mu_{\rm max} - \mu$ below T_g for all Δt's. As seen from the inset of Fig. 6, $\mu_{\rm med} - \mu$ has a peak similar to $\delta\mu$ becoming sharper with an increasing Δt.

Summary.—We investigated by means of MD simulations a coarse-grained model for polymer glasses characterizing its shear modulus μ using the stress-fluctuation formalism. The observed Δt dependence of μ (Fig. 1) and its contributions μ_1 and μ_F can be traced back to the finite time (time-averaged) stress fluctuations' need to explore the phase space which is perfectly described (Fig. 4) by the weighted integral over the shear-stress relaxation modulus $G(t)$ [Eq. (4)]. The liquid-solid transition characterized by the ensemble-averaged $\mu(T)$ is continuous for all sampling times Δt, but it becomes sharper—and thus better defined—with an increasing Δt (Fig. 1). However, while the transition gets more steplike *on average*, increasingly strong fluctuations between different configurations underly the transition. The broad and lopsided distribution $p(\bar{\mu})$ below T_g makes the prediction of the modulus $\bar{\mu}$ of a single configuration elusive (Fig. 6).

Beyond the current study.—While μ and its contributions μ_A, μ_F, μ_0, and μ_1 do not depend on the system size [29], this is more intricate for the corresponding standard deviations and must be addressed in the future following Ref. [20]. Recent work on self-assembled networks [21] suggests that $\delta\mu \approx \delta\mu_F \sim 1/\sqrt{V}$ for $T \ll T_g$ (self-averaging), while $\delta\mu \approx \delta\mu_F \sim V^0$ around T_g (lack of self-averaging). In the latter limit, long-range elastically interacting activated events are expected to dominate the plastic reorganizations of the particle contacts [43]. From a broader vantage point, it is no surprise that the lifting of the permutation invariance of the liquid state below T_g [5] should lead to strong fluctuations between different configurations. The observation of strong frozen-in shear stresses (Figs. 2 and 3) is thus merely a demonstration of the broken symmetry. Analysis tools need to account for these frozen zero-wave-vector stresses, and theoretical approaches neglecting them are bound to miss the heart of the problem.

I. K. thanks the IRTG Soft Matter for their financial support. We are indebted to O. Benzerara (ICS, Strasbourg) and H. Xu (Metz) for the helpful discussions. We thank the University of Strasbourg for a generous grant of CPU time through GENCI/EQUIP@MESO.

*joachim.wittmer@ics-cnrs.unistra.fr

[1] L. D. Landau and E. M. Lifshitz, *Theory of Elasticity* (Pergamon Press, New York, 1959).
[2] M. Doi and S. F. Edwards, *The Theory of Polymer Dynamics* (Clarendon Press, Oxford, 1986).
[3] J. Hansen and I. McDonald, *Theory of Simple Liquids*, 3rd ed. (Academic Press, New York, 2006).
[4] M. Rubinstein and R. Colby, *Polymer Physics* (Oxford University Press, Oxford, 2003).
[5] S. Alexander, Phys. Rep. **296**, 65 (1998).
[6] D. Li, H. Xu, and J. P. Wittmer, J. Phys. Condens. Matter **28**, 045101 (2016).
[7] J.-L. Barrat, J.-N. Roux, J.-P. Hansen, and M. L. Klein, Europhys. Lett. **7**, 707 (1988).
[8] H. Yoshino, J. Chem. Phys. **136**, 214108 (2012).
[9] A. Zaccone and E. M. Terentjev, Phys. Rev. Lett. **110**, 178002 (2013).
[10] J. P. Wittmer, H. Xu, P. Polińska, F. Weysser, and J. Baschnagel, J. Chem. Phys. **138**, 12A533 (2013).
[11] W. Götze, *Complex Dynamics of Glass-Forming Liquids: A Mode-Coupling Theory* (Oxford University Press, Oxford, 2009).
[12] G. Szamel and E. Flenner, Phys. Rev. Lett. **107**, 105505 (2011).
[13] M. Ozawa, T. Kuroiwa, A. Ikeda, and K. Miyazaki, Phys. Rev. Lett. **109**, 205701 (2012).
[14] C. L. Klix, F. Ebert, F. Weysser, M. Fuchs, G. Maret, and P. Keim, Phys. Rev. Lett. **109**, 178301 (2012).
[15] C. L. Klix, G. Maret, and P. Keim, Phys. Rev. X **5**, 041033 (2015).
[16] H. Yoshino and F. Zamponi, Phys. Rev. E **90**, 022302 (2014).
[17] A. Andreanov, G. Biroli, and J.-P. Bouchaud, Europhys. Lett. **88**, 16001 (2009).
[18] P. Charbonneau, J. Kurchan, G. Parisi, P. Urbani, and F. Zamponi, Nat. Commun. **5**, 3725 (2014).
[19] G. Biroli and P. Urbani, Nat. Phys. **12**, 1130 (2016).

[20] I. Procaccia, C. Rainone, C. A. B. Z. Shor, and M. Singh, Phys. Rev. E **93**, 063003 (2016).
[21] J. P. Wittmer, I. Kriuchevskyi, A. Cavallo, H. Xu, and J. Baschnagel, Phys. Rev. E **93**, 062611 (2016).
[22] D. Montarnal, M. Capelot, F. Tournilhac, and L. Leibler, Science **334**, 965 (2011).
[23] M. Allen and D. Tildesley, *Computer Simulation of Liquids* (Oxford University Press, Oxford, 1994).
[24] S. J. Plimpton, J. Comput. Phys. **117**, 1 (1995).
[25] S. Frey, F. Weysser, H. Meyer, J. Farago, M. Fuchs, and J. Baschnagel, Eur. Phys. J. E **38**, 11 (2015).
[26] J. Baschnagel, I. Kriuchevskyi, J. Helfferich, C. Ruscher, H. Meyer, O. Benzerara, J. Farago, and J. Wittmer, in *Polymer Glasses*, edited by C. Roth (Taylor & Francis, London, 2016), p. 153.
[27] B. Schnell, H. Meyer, C. Fond, J. P. Wittmer, and J. Baschnagel, Eur. Phys. J. E **34**, 97 (2011).
[28] I. Kriuchevskyi, J. Wittmer, O. Benzerara, H. Meyer, and J. Baschnagel, Eur. Phys. J. E **40**, 43 (2017).
[29] See Supplemental Material at http://link.aps.org/supplemental/10.1103/PhysRevLett.119.147802 for details concerning the model Hamiltonian, the quench protocol, and the data sampling (Sec. I), the connection between canonical affine shear transformations and the instantaneous shear stress $\hat{\tau}$ and the affine shear modulus $\hat{\mu}_A$ (Sec. II), the determination of the shear-stress relaxation modulus $G(t)$ for solidlike systems with quenched shear stresses (Sec. III), and the derivation of Eq. (4) for systems with time-translational invariance (Sec. IV). A summary of ongoing work on system-size effects is given in Sec. V.
[30] J. P. Wittmer, A. Tanguy, J.-L. Barrat, and L. Lewis, Europhys. Lett. **57**, 423 (2002).
[31] J.-L. Barrat, in *Computer Simulations in Condensed Matter Systems: From Materials to Chemical Biology—Vol. 2*, edited by M. Ferrario, G. Ciccotti, and K. Binder, Lecture Notes in Physics Vol. 704 (Springer, Berlin, 2006), p. 287.
[32] H. Xu, J. P. Wittmer, P. Polińska, and J. Baschnagel, Phys. Rev. E **86**, 046705 (2012).
[33] D. R. Squire, A. C. Holt, and W. G. Hoover, Physica (Amsterdam) **42**, 388 (1969).
[34] J. F. Lutsko, J. Appl. Phys. **64**, 1152 (1988).
[35] J. P. Wittmer, H. Xu, and J. Baschnagel, Phys. Rev. E **91**, 022107 (2015).
[36] J. P. Wittmer, H. Xu, O. Benzerara, and J. Baschnagel, Mol. Phys. **113**, 2881 (2015).
[37] J. P. Wittmer, I. Kriuchevskyi, J. Baschnagel, and H. Xu, Eur. Phys. J. B **88**, 242 (2015).
[38] J. P. Wittmer, H. Xu, and J. Baschnagel, Phys. Rev. E **93**, 012103 (2016).
[39] $\langle \cdots \rangle$ denotes an ensemble average over configurations and shear planes.
[40] μ_A and μ_0 are, in this sense, static observables. The observation that μ_A and μ_0 systematically deviate below T_g (Fig. 2) thus implies that the glass transition of our polymer melts cannot be interpreted in terms of a purely dynamical theoretical framework.
[41] D. P. Landau and K. Binder, *A Guide to Monte Carlo Simulations in Statistical Physics* (Cambridge University Press, Cambridge, England, 2000).
[42] For $T > T_g$, the distribution is Gaussian, centered at a maximum $\mu_{\max} = 0$ and getting sharper with increased sampling time Δt (not shown).
[43] E. E. Ferrero, K. Martens, and J.-L. Barrat, Phys. Rev. Lett. **113**, 248301 (2014).